Optical Materials 146 (2023) 114610

Contents lists available at ScienceDirect

Optical Materials

journal homepage: www.elsevier.com/locate/optmat

Research Article

Electromagnetic wave propagation in cylindrical photonic crystals with engineered disorder effects

Jia-Tao Zhang, Si-Si Rao, Hai-Feng Zhang *

College of Electronic and Optical Engineering & College of Flexible Electronics (Future Technology), Nanjing University of Posts and Telecommunications, Nanjing, 210023, China

ARTICLE INFO

Keywords:
Cylindrical photonic crystals
Photonic band gaps
Transmission spectrum
Disorder
Transfer matrix method

ABSTRACT

In this study, the manipulation of engineered disorder effects in cylindrical photonic crystals is examined, with a focus on the influence of three varied types of disorder effects on the transmission spectra near the first five photonic band gaps of CPCs. The investigation employed the basic $(ABA)^N$ model, where A and B depict two isotropic dielectrics, and N is the number of periods. The impact of the disorder on the CPCs is analyzed and discussed in detail. In addition, the disorder-induced localization and delocalization of the electromagnetic waves are measured by the inverse participation rate and disorder-to-order energy ratio. These results are analyzed numerically. Based on this, the intrinsic connection between the defined parameters and the mechanism of disorder-influenced structure switching between the localized and transmitted states is investigated. All the above phenomena and findings might lead to a new understanding of electromagnetic wave transmission and localization in micro and nano-optical devices.

1. Introduction

Photonic crystals (PCs) [1–5] are a new type of structure composed of a periodic arrangement of dielectrics, the most important feature of which is that they have forbidden bands similar to that in the energy band structures of semiconductors, which is called the photonic band gaps (PBGs). Depending on the arrangement coordinate system, one-dimensional (1-D) PCs can also be separated into planar PCs, cylindrical photonic crystals (CPCs) [6–9], and sphere photonic crystals (SPCs) [10,11]. Many research teams are focusing on CPCs as a "stepping stone" between planar PCs and SPCs. The propagation properties of electromagnetic (EM) waves in the CPCs can be derived using the transfer matrix method (TMM) [12,13] expanded on a cylindrical coordinate system, the same as in 1-D planar PCs [14]. Theoretically, many of the intriguing phenomena discovered in a 1-D planar PC model might be observed in a CPC using a comparable model. In 2013, in the work of Hu et al. [13] on the derivation of a TMM applicable to CPCs, the reflection spectra calculated by this method expressed the same PBGs as the 1-D planar structure. Similarly, the effect of defective modes on the transmission characteristics of CPCs, discussed by El-Naggar [8] in 2020, succeeded in obtaining sharp transmission peaks at the forbidden band, which is similar to the results obtained using plane waves. It must be admitted that the transition from a plane coordinate system to a cylindrical coordinate system, and eventually to a spherical coordinate system, is an unavoidable trend and a required route for this area of research and that present and future scholars will continue to move forward on this path.

Despite the increasing maturity of nanofabrication technology in the processing of PCs structures, disorder effects are still inevitable in the fabricated devices, and this imperfection leads to a significant deterioration of their optical properties when compared to theoretical values. Since Sajeev John first proposed in 1987 the possibility that the introduction of disorder in PCs could manipulate the local density of optical states [15], over the decades, a considerable body of study based on 1-D planar PCs [16–18] has emerged, leading to a number of commonly accepted results. It has been demonstrated that disorder effects have the capacity to force light to shift between localization and nonlocalization, notably in the PBGs' proximity [19–21]. The tail of the density of states in the passband has also been discovered to be the primary driver of local relaxation in the PBG. Furthermore, when the disorder level exceeds a certain threshold, the density of states can be detected in the middle of PBG [20]. Following that, teams conducted systematic studies using 1-D planar PCs to manipulate the transmission and localization of EM waves via disorder effects [16]. The superior qualities of the disorder

* Corresponding author.
E-mail addresses: hanlor@163.com, hanlor@njupt.edu.cn (H.-F. Zhang).

https://doi.org/10.1016/j.optmat.2023.114610
Received 13 September 2023; Received in revised form 21 October 2023; Accepted 8 November 2023

effect in managing EM wave transmission make it an unavoidable new concept for optical focusing [22], filters [23], optical data storage [24], and other applications. In 2021, Sharabi et al. [25] introduced disorder into photonic time crystals, and studied the propagation of EM waves in this medium, and showed that the exponential decrease in group velocity and the exponential increase in the amplitude of pulse propagation depended strongly on the Floquet band structure of the photonic time crystals. In 2022, Rout et al. [26] investigated the transport properties of light through polymer PCs using the thickness of the dielectric layer as a disorder, and discovered the robustness of this structure over a large disorder range, elucidating its potential application in integrated photonic devices and optical communication systems. Parient et al. [27] observed the transition of light propagation from total reflection to enhanced transmission in vacancy-doped PCs and explained this peculiar phenomenon with the help of the principle of Fano-like resonance. There is never-ending research on the disorder in PCs. But until now, few researchers have concentrated on the numerous features of disorder effects in the cylindrical coordinate system.

In this work, by designing the basic structure and introducing two parameters to numerically analyze the simulation results for three different refractive-index-disorder cases in various aspects, we are the first to investigate the role of disorder effects on the control of EM waves in the CPCs. The typical scenarios of disorder-induced propagation found during the simulation are depicted in Fig. 1, where the four curves show the dependence between transmittance and disorder intensity σ at different angular frequencies. The green line 4 indicates a significant decrease in transmittance with the enhancement of disorder introduction. The blue line 2 corresponds to the case where the introduction of disorder leads to a sudden increase in the transmittance of the band that was originally in the PBG. In addition to the above two transmission scenarios that are most typical in disordered, there are two more unusual novel transmission options: the red line 1, where the transmittance is unaffected by the degree of disorder and remains high. The orange line 3, whose phenomenon is similar to line 4 when weakly disordered, decays at a much greater rate than it, and the transmittance dramatically rises back to a certain level when the disorder strength exceeds a threshold. On this foundation, we investigated the effects of the disorder effect using the electric field energy ratio and standard deviation of each dielectric layer with and without the disorder. These details are crucial for understanding EM wave propagation and localization in the CPCs.

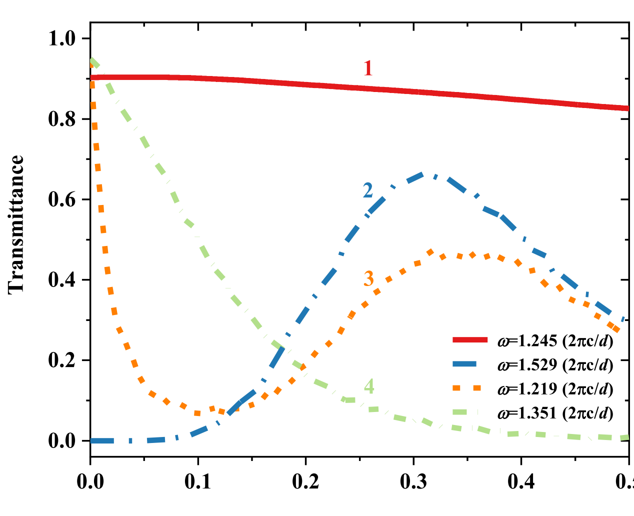

Fig. 1. The diagram of four typical cases of disorder-induced propagation in CPCs versus disorder intensity.

2. Structure design and simulation

Fig. 2 depicts the structure employed in this paper, A and B are two general isotropic dielectrics with thicknesses and relative permittivities represented by d_A, d_B, ε_A, and ε_B, respectively. One period of the CPCs is an ABA structure composed of two layers of dielectric A and one layer of dielectric B with its thickness $d = 2d_A + d_B$, and N denotes the number of periods of the whole structure. The model's center is filled with air, and the tubular body's inner radius is represented by ρ_0, $\rho_f = \rho_0 + N \times d$ denotes the outermost radius of the structure. By the way, the value of ρ_0 in Fig. 2 is taken to be on the small side to clearly highlight the underlying structure of the model. The transfer matrix method [12,13] will be used to depict the propagation properties of EM waves in this construction.

In general, the two curl equations of Maxwell's equations have the following forms:

$$\nabla \times \boldsymbol{E} = -\mathrm{i}\omega\mu\boldsymbol{H}, \tag{1}$$

$$\nabla \times \boldsymbol{H} = \mathrm{i}\omega\varepsilon\boldsymbol{E}. \tag{2}$$

Expanding them on the cylindrical coordinate system and assuming that the EM wave is incident in the TM mode, after keeping the non-zero variables H_z, E_ρ, E_φ, Eqs. (1) and (2) can be combined to generate the following equation system:

$$\frac{1}{\rho}\frac{\partial H_z}{\partial \varphi} = \mathrm{i}\omega\varepsilon E_\rho, \tag{3a}$$

$$\frac{\partial H_z}{\partial \rho} = -\mathrm{i}\omega\varepsilon E_\varphi, \tag{3b}$$

$$\frac{1}{\rho}\left[\frac{\partial(\rho E_\varphi)}{\partial \rho} - \frac{\partial E_\rho}{\partial \varphi}\right] = -\mathrm{i}\omega\mu H_z. \tag{3c}$$

Eliminating the variables E_ρ and E_φ from Eq. (3) yields an equation relating only to H_z:

$$\rho\frac{\partial}{\partial \rho}\left(\rho\frac{\partial H_z}{\partial \rho}\right) - \frac{\rho^2}{\varepsilon}\frac{\partial \varepsilon}{\partial \rho}\frac{\partial H_z}{\partial \rho} + \frac{\partial}{\partial \rho}\frac{\partial H_z}{\partial \varphi} + \omega^2\mu\varepsilon\rho^2 H_z = 0. \tag{4}$$

Using the separation of variables method, the solution of the above-complicated equation can be easily provided in the form of

$$H_z(\rho,\varphi) = V(\rho)\Phi(\varphi) = [A\mathrm{J}_m(k\rho) + B\mathrm{Y}_m(k\rho)]e^{im\varphi}, \tag{5}$$

where m is the azimuthal number, J_m and Y_m are the Bessel function and Neumann function with constant coefficients A and B, respectively, and $k = \omega(\mu\varepsilon)^{1/2}$ is the EM wave vector. Substituting Eq. (5) into Eq. (3b) can express the solution of E_φ in a similar form:

$$\mathrm{E}_\varphi(\rho,\varphi) = U(\rho)\Phi(\varphi) = \mathrm{i}p\left[A\mathrm{J}_m^{'}(k\rho) + B\mathrm{Y}_m^{'}(k\rho)\right]e^{\mathrm{i}\omega\varphi}, \tag{6}$$

where $p = (\mu/\varepsilon)^{1/2}$, $\mathrm{J}_m^{'}$ and $\mathrm{Y}_m^{'}$ are the derivatives of the Bessel and Neumann functions. Based on the conclusions of Eqs. (5) and (6), a second-order matrix $\boldsymbol{M}$ can be built to relate the relationship between H_z and E_φ when ρ takes different values and it takes the following shape:

$$\begin{bmatrix} V(\rho) \\ U(\rho) \end{bmatrix} = \boldsymbol{M}\begin{bmatrix} V(\rho_0) \\ U(\rho_0) \end{bmatrix}. \tag{7}$$

When the four elements of the matrix $\boldsymbol{M}$ are represented by mm_{11}, mm_{12}, mm_{21}, and mm_{22}, respectively, their values are deduced to be [13].

$$mm_{11} = \frac{\pi}{2}k\rho_0\left[\mathrm{Y}_m^{'}(\mathrm{k}\rho_0)\mathrm{J}_m(\mathrm{k}\rho) - \mathrm{J}_m^{'}(\mathrm{k}\rho_0)\mathrm{Y}_m(\mathrm{k}\rho)\right], \tag{8a}$$

$$mm_{12} = -\mathrm{i}\frac{\pi}{2}\frac{k}{p}\rho_0[\mathrm{Y}_m(\mathrm{k}\rho)\mathrm{J}_m(\mathrm{k}\rho_0) - \mathrm{J}_m(\mathrm{k}\rho)\mathrm{Y}_m(\mathrm{k}\rho_0)], \tag{8b}$$

$$mm_{21} = -\mathrm{i}\frac{\pi}{2}kp\rho_0\left[\mathrm{Y}_m^{'}(\mathrm{k}\rho_0)\mathrm{J}_m^{'}(\mathrm{k}\rho) - \mathrm{J}_m^{'}(\mathrm{k}\rho_0)\mathrm{Y}_m^{'}(\mathrm{k}\rho)\right], \tag{8c}$$

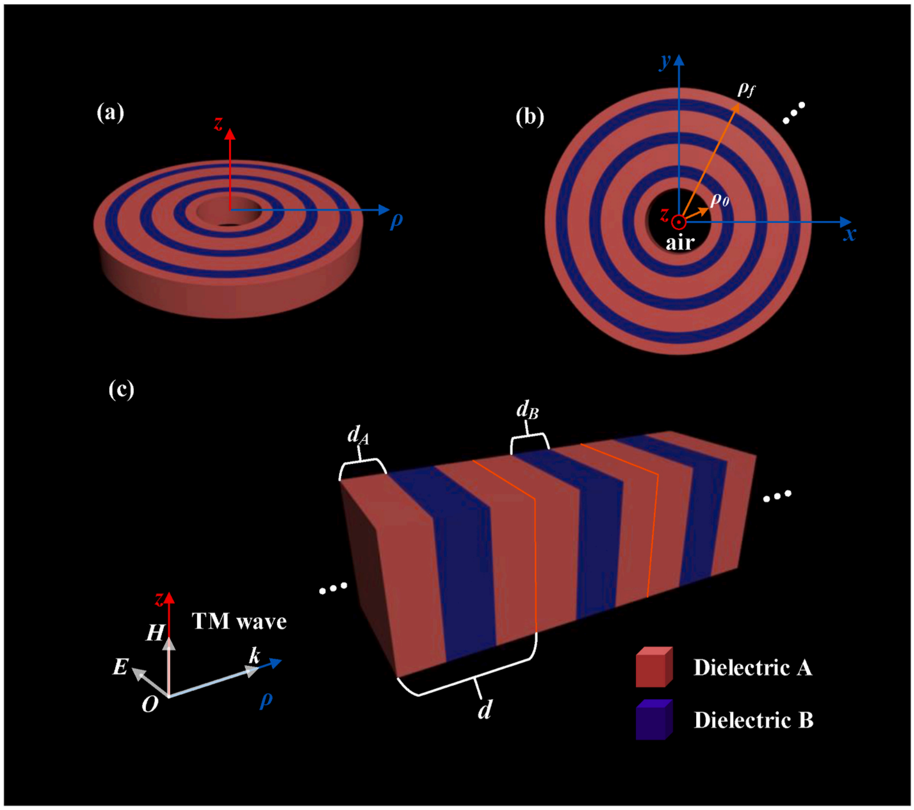

Fig. 2. Schematic diagram of CPCs with $(ABA)^N$ structure consisting of dielectrics A and B, where N is the number of periods, (a) Stereogram of the model, (b) Top view of the model, and (c) Sectional view of the model.

$$mm_{22} = \frac{\pi}{2} k\rho_0 \left[Y_m'(k\rho) J_m(k\rho_0) - J_m'(k\rho) Y_m(k\rho_0) \right], \tag{8d}$$

where the inner and outer radii of a single cylindrical dielectric slab are denoted by ρ_0 and ρ, respectively. The transmission characteristics of the cylindrical wave in the whole structure are the result of the cumulative multiplication of the transfer matrix of each layer, in turn, take the example of a cylindrical wave diverging from the center outward,

$$\boldsymbol{M} = \boldsymbol{M}_1 \boldsymbol{M}_2 \boldsymbol{M}_3 \cdots \boldsymbol{M}_{(3N-2)} \boldsymbol{M}_{(3N-1)} \boldsymbol{M}_{3N}. \tag{9}$$

After further computations, the formulations of transmission coefficients can be produced in the form of [13].

$$t_d = \frac{4\sqrt{\varepsilon^- / \mu^-}}{\pi K \rho^- H_m^2(k^- \rho^-) H_m^1(k^- \rho^-) \left[-\left(ip^- C_{m-}^1 M_1' + M_3' \right) + ip^+ C_{m+}^2 \left(ip^- C_{m-}^2 M_2' + M_4' \right) \right]}, \tag{11}$$

where the elements of the inverse matrix of $\boldsymbol{M}$ are denoted by M_1', M_2', M_3', and M_4', and the subscripts - and + refer to the incident surface and the exit surface, respectively. $H_m^{1,2}$ and $H_m'^{1,2}$ are the first or the second Hankel functions and their derivatives, and

$$C_{ml}^{1,2} = \frac{H_m'^{1,2}(k_l \rho_l)}{H_m^{1,2}(k_l \rho_l)}, (\text{lis-or} +). \tag{12}$$

The transmittance are equal to the square of the modes of the transmission coefficients:

$$T = |t_d|^2. \tag{13}$$

3. Analysis and discussion

Let $d_A = 0.32d$, $d_B = 0.36d$, initial radius $\rho_0 = 10000d$ and $N = 500$ be the number of periods, and the expectation of the relative permittivity of the dielectrics A and B be $\bar{\varepsilon}_A = 2.6$ and $\bar{\varepsilon}_B = 2.8$, respectively, using the structure given in Fig. 2. In this paper, we provide three different forms of disorder to examine their consequences on the structure. In the first, the disorder is introduced into the dielectric A, causing its relative permittivity to follow a normal distribution with mean $\bar{\varepsilon}_A$ and standard deviation σ_A, while the dielectric B's relative permittivity remains constant at $\bar{\varepsilon}_B$. The second case, like the first, retains the dielectric A's relative permittivity at $\bar{\varepsilon}_A$ while creating disorder in the dielectric B layer, causing its relative permittivity to obey a mean value of $\bar{\varepsilon}_B$ and a standard deviation of σ_B with a normal distribution. In the third scenario, the disorder is introduced in both dielectric A and dielectric B, and the relative permittivity of each dielectric follows a normal distribution, with the expected value as the mean and the σ as the standard deviation. In these three disorder situations, the random process is sampled for several times $H = 1000$, and the TMM is utilized to focus on the transmission of the cylindrical wave at the first five PBGs. Taking the second type of disorder case as an example, the relative permittivity distribution of CPCs in the ρ-direction at different disorder intensities is shown in Fig. 3.

It is well known that when no disorder is added, the center frequency

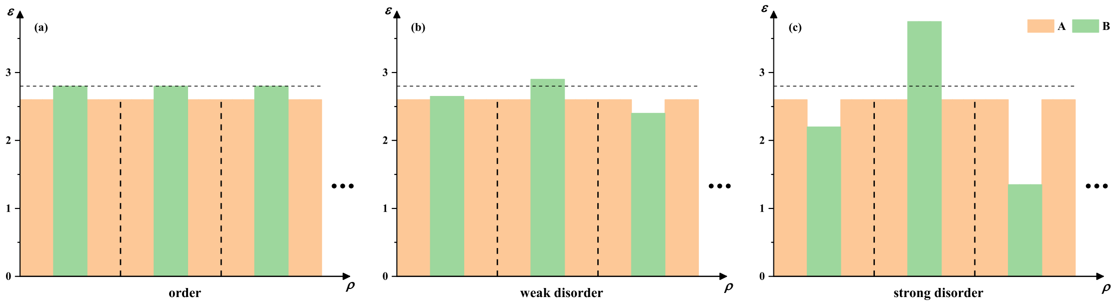

Fig. 3. Introducing the statistical mean of the relative permittivity distribution in the layer B for different disorder strengths σ, (a) order, (b) weak disorder and (c) strong disorder.

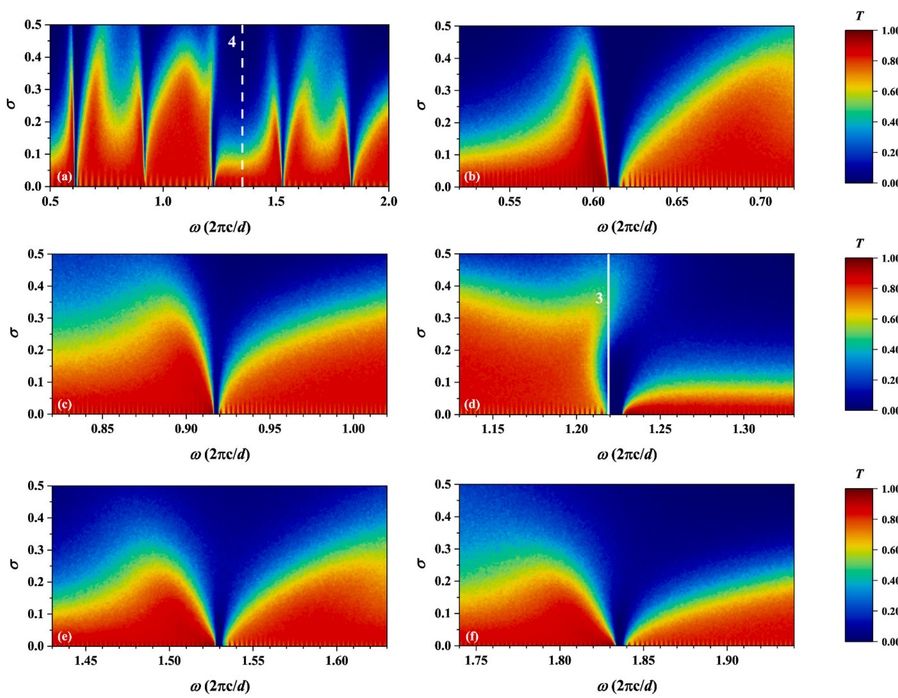

Fig. 4. The transmission spectra in the first case of disorder introduction, where only the relative permittivity of the dielectric A revolves around $\overline{\varepsilon}_A$ fluctuates, $\sigma_A = \sigma$, (a) transmission spectra of cylindrical wave frequency at 0.5–2 (2πc/d), (b)~(f) transmission spectra of cylindrical wave frequencies around each PBGs at 0.5–2 (2πc/d).

ω_l of the lth order PBG of the PCs structure fulfills [17].

$$\frac{\omega_l \overline{n} d}{c}, l = 1, 2, \ldots \tag{14}$$

where the average refractive index is $\overline{n} = (2d_A\sqrt{\overline{\varepsilon}_A} + d_B\sqrt{\overline{\varepsilon}_B})/\ d$ for the structure of $(ABA)^N$. When the frequency of the cylindrical wave falls within a particular range around this frequency, its propagation through the PCs is restricted, and conversely, when the frequency is far from ω_l, it can travel through the structure practically completely. However, this phenomenon changes when the disorder is introduced into the structure.

Fig. 4 reveals the results of the first disorder introduction case. Generally speaking, the introduction of disorder will result in a reduction in the structure's transmittance, and these phenomena can become more obvious as the disorder strength steadily rises, as shown by dashed line 4 in Fig. 4(a). However, several odd variations in the transmittance of the structure with increasing disorder strength can still be observed in some other regions of the transmission spectra. The transmittance of the structure in the disorder-free state can be up to 0.945 for the case shown in solid line 4 of Fig. 4(d), and the value will decrease sharply in the weakly disordered case until it reaches a minimum value of 0.068 at σ=0.13 (This attenuation appears to be even more drastic than that represented by the dashed line 4). When the magnitude of σ is further increased, the transmittance gradually returns to 0.477 at σ=0.32 and eventually exhibits a decreasing trend, which means that the opaque properties expressed by the structure under weak disorder will be transformed into translucency as strong disorder is introduced.

As seen in Fig. 5, the structure is more resistant to the second class of disorder introduction scenarios compared to the first type, which is most likely caused by the fact that dielectric B occupies a smaller proportion of the whole structure. This is manifested in the fact that a portion of the original passband under strong disorder can still maintain a certain value of transparency to EM waves. It is even possible to perceive a special case of transmission as shown by the solid line 1 in Fig. 5(d). In this condition, the structure reflects extreme robustness to disorder, and the transmittance under strong disorder ($T = 0.8259$) still reaches 91.44 % of what it would have been without the introduction of disorder ($T = 0.9032$). The one depicted by dashed line 2 in Fig. 5(e) is another case, where the forbidden band in the ordered situation instead induces a transmission upon the addition of disorder, which can reach a maximum of 0.6655 at $\sigma = 0.31$.

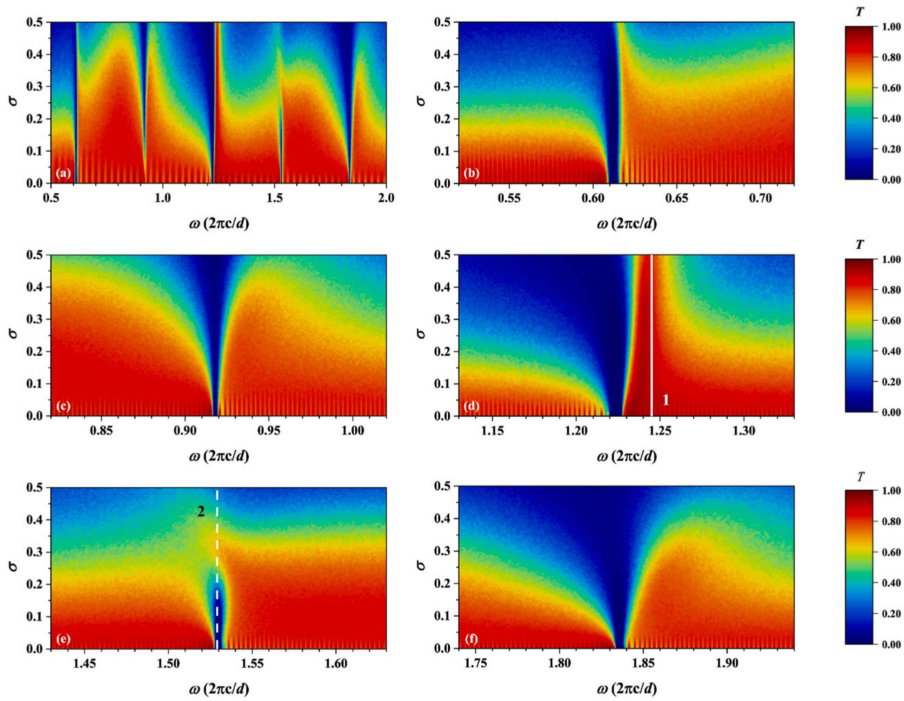

Fig. 5. The transmission spectra in the second case of disorder introduction, where only the relative permittivity of the dielectric B revolves around $\bar{\varepsilon}_B$ fluctuates, $\sigma_B = \sigma$, (a) transmission spectra of cylindrical wave frequency at 0.5–2 (2πc/d), (b)~(f) transmission spectra of cylindrical wave frequencies around each PBGs at 0.5–2 (2πc/d).

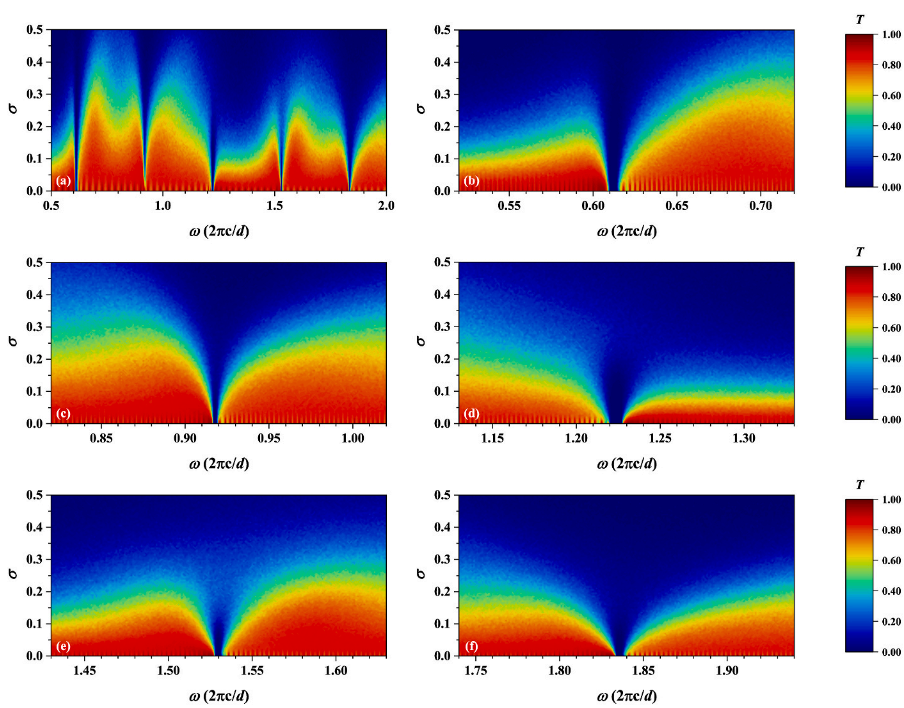

Fig. 6. The transmission spectra in the third case of disorder introduction, where the relative permittivity of the dielectric A and B revolve around $\bar{\varepsilon}_A$ and $\bar{\varepsilon}_B$ fluctuate, respectively, $\sigma_A = \sigma_B = \sigma$, (a) transmission spectra of cylindrical wave frequency at 0.5–2 (2πc/d), (b)~(f) transmission spectra of cylindrical wave frequencies around each PBGs at 0.5–2 (2πc/d).

For the third type of case where both layers A and B are introduced into disorder, as shown in Fig. 6, the variation of transmittance with disorder intensity in all passband and forbidden band regions has a similar trend. It can be easily concluded that the structure is most sensitive to this type of disorder so that at disorder strength $\sigma = 0.4$, the structure's transmittance for all EM waves in the range 0.5–2 (2πc/d) is only 0.0312 on average. This undifferentiated opacity to EM waves over the entire interval is one of the characteristics of the third type of disordered scenario.

To numerically analyze the manipulation of cylindrical waves by disorder effects, the structure exhibited in Fig. 2 will continue to be used to compare the four typical cases of disorder shown in Fig. 1. The number of periods of the structure is 500, so that the thickness of the structure in the direction of EM wave propagation is 500*d*. Of the four curves shown in Fig. 1, curves 1 and 2 employ the second type of disorder introduction, i.e., only the dielectric layer B has been introduced into the disorder, while the other curves 3 and 4 exist when the first type of disorder is introduced. Now, we define the inverse participation ratio [28].

$$P = \frac{\int I^2(\rho)\mathrm{d}\rho}{\left(\int I(\rho)\mathrm{d}\rho\right)^2} \tag{15}$$

to quantify the degree of localization of EM waves in CPCs, where the light intensity I is numerically proportional to the square of the electric field strength $|E|$. Further, the effective propagation length L_{eff} is defined as [28].

$$L_{eff} = \langle P \rangle^{-1}, \tag{16}$$

where the pointed brackets (<> in Eq. (16)) indicate the mean value after multiple sampling, the thickness d of a single cell is 80 μm, which means the thickness of the whole structure is 40 mm, and the number of realizations $H = 1000$. At angular frequencies, $\omega = 1.245$ ($2\pi c/d$) and 1.529 ($2\pi c/d$), respectively, Fig. 7(b) and (g) illustrate the relationship between the mean value of the inverse participation rate and the disorder intensity σ, while Fig. 7(c) and (h) show the corresponding effective propagation lengths. The average inverse participation ratio at the passband is mainly below 40 m^{-1} when no disorder is introduced, and the effective propagation length is more than 0.025 m, implying that the structure is practically transparent to EM waves. As σ increases, $<P>$ and L_{eff} at $\omega = 1.245$ ($2\pi c/d$) do not change drastically, and the effective propagation length continues to remain above 0.025 m, demonstrating the high stability at this point for disordered. The curve in Fig. 7(g) decreases rapidly between $\sigma = 0.05$–0.2, corresponding to the rising transmittance in its transmission spectrum. As a result, a very modest change in the disorder intensity can cause a transition between the two states of the cylindrical wave in the local and propagation domains in these circumstances. In addition, the disorder-to-order energy ratio [16].

$$R = \frac{\int_{\varepsilon=\varepsilon_{id}} \varepsilon(\rho)|E(\rho)|^2\mathrm{d}\rho}{\int_{\varepsilon=\varepsilon_{io}} \varepsilon(\rho)|E(\rho)|^2\mathrm{d}\rho}, (i = \mathrm{A}, \mathrm{B}) \tag{17}$$

is introduced in this work to reflect the variation law of electric field energy under different disorder intensities, where ε_{id} is the relative permittivity of the dielectric A and B after the introduction of disorder, while ε_{io} is their relative permittivity in the ordered case. In other words, $\varepsilon_{\mathrm{Ad}} = \varepsilon_{\mathrm{Ao}}$ for the curves 3 and 4 in Fig. 1, while the curves 1 and 2 are $\varepsilon_{\mathrm{Bd}} = \varepsilon_{\mathrm{Bo}}$. As shown in Fig. 7(d) and (i), the average values of the disorder ratios of layers A and B at two angular frequencies are expressed by the blue and red dots, respectively, with the same number of sampling times of 1000. Clearly, when $\sigma = 0$, $<R>$ is 1. As shown in Fig. 7(a), the disorder-to-order energy ratio fluctuates steadily around 1 in both A and B layers, which implies that the introduction of disorder hardly affects the intensity distribution of EM waves in the structure. This also explains why the transmittance of the structure can be maintained at a high level at this frequency point. It can be inferred that the disorder intensity threshold in this situation is quite high, and that σ must reach a pretty high level to have a substantial influence on the localization and propagation state of EM waves, which is a highly unique case. In contrast, Fig. 7(i) shows that the localization of the structure to the field under strong disorder at $\omega = 1.529$ ($2\pi c/d$) is only 0.5–0.7 times as large as in

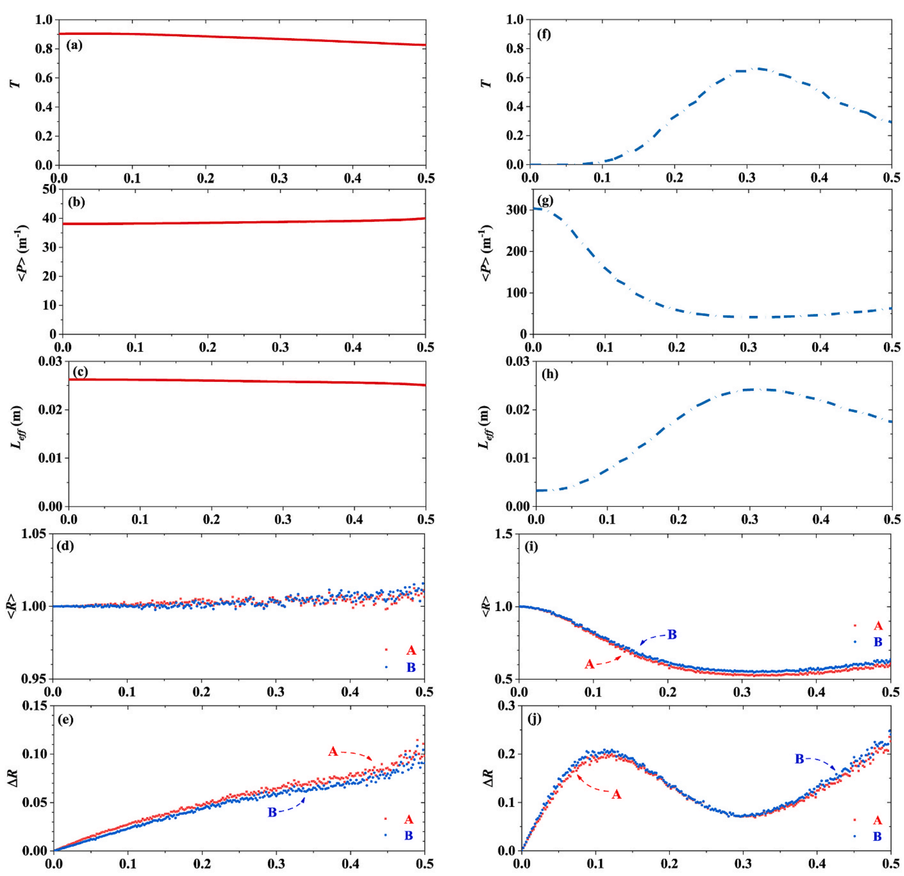

Fig. 7. Relationships between transmission T, inverse participation ratio $<P>$, effective propagation length L_{eff}, disorder-to-order energy ratio $<R>$, standard deviation of disorder-to-order energy ratio ΔR and disorder intensity σ at different angular frequencies, (a)~(e) $\omega = 1.245$ ($2\pi c/d$) and (f)~(i) $\omega = 1.529$ ($2\pi c/d$).

order, reflecting the transmittance properties expressed by the structure in the transmission curve as σ increases. On this premise, we also address the standard deviation of R for various disorder intensities, represented by ΔR in Fig. 7(e) and (j). For the case of $\omega = 1.245$ ($2\pi c/d$), ΔR becomes larger only slowly as the disorder strength increases, since the overall transmission characteristics do not change significantly. In contrast, in Fig. 7(j), σ at less than 0.11, the increasing ΔR corresponds to the transition of the electromagnetic wave between localization and delocalization. This evolution implies that as the disorder strength σ increases, the random coherent scattering becomes weaker and the propagation of the light is enhanced. At $\sigma \sim 0.3$, the dispersed ΔR indicates a change in transmission mode and ultimately decreases the transmittance towards 0.

Similarly, Fig. 8 depicts the graphs of the different parameters for the other two examples in Fig.1, Figs.8(a)~(e) correspond to $\omega = 1.219$ ($2\pi c/d$), whereas Fig. 8(f)~(i) correspond to $\omega = 1.351$ ($2\pi c/d$). The same analytical approach can be applied to comprehend the computations for the two situations highlighted in Fig. 8, as it was for the first two disorders. First, in the instance of $\omega = 1.219$ ($2\pi c/d$), the images of both <P> and L_{eff} reflect to some extent the trend of the transmission spectrum. At $\sigma = 0.13$, <P> and L_{eff} reach the maximum and minimum points, respectively, corresponding to the rapid decay of transmittance in the introduction of weak disorder. In Fig. 8(d), the slight decrease in the disorder-to-order energy ratio in both the A and B layers after $\sigma > 0.13$ provides the basis for a rebound in T and the effective propagation length. For the angular frequency $\omega = 1.351$ ($2\pi c/d$), the transmittance continues to decrease and approximates to 0 at strong disorder, as seen in Fig. 8(a). This distribution of transmittance is undoubtedly the most prevalent transmission pattern under disorder, and as the disorder intensity increases to 0.24, the transmittance becomes only 0.1052. Fig. 8 (d) and (i) display two instances where <R> exceeds 1, signifying that transmittance ought to be lower than the ordered situation. However, in the interval of $\sigma = 0.14$ to 0.35, a slight decrease in <R> can account for the transmission window, with $\omega = 1.219$ ($2\pi c/d$). Another point worth noting is that the magnitude of <R> in the two dielectrics is strikingly similar. In the scenarios illustrated in Fig. 7(i) and 8(d), the change in the energy ratio of layer A is generally larger than that of layer B, making it easier to assume that the influence of layer A on the structure occupies a larger portion. Fig. 8(i), on the other hand, shows that in general layers A and B seem to manipulate the transmission characteristics of the structure with considerable weight. Furthermore, the standard deviation of the disorder-to-order energy ratio, in particular, as shown in Fig. 8(e) and (j), follows a similar pattern to that of <P>.

Based on the data displayed in Figs. 7 and 8, it can be observed that the four parameters, namely <P>, L_{eff}, <R>, and ΔR, exhibit certain responsiveness to the shift in structure from localization and delocalization when disorder is introduced. In particular, when the effective propagation length approaches the structure length, a larger proportion of electromagnetic energy can pass through, and vice versa for <P>, as it is inversely proportional to L_{eff}. The value of <R> indicates the ratio of energy that remains confined within the structure when the disorder is introduced compared to the ordered state. If <R> is greater than 1, it suggests that the transmission mode is more likely to be concentrated locally. On the other hand, a ratio less than 1 indicates that the transmittance is boosted relative to the ordered scenario. The inflection point of the variance of R corresponds to the boundary of the transition between the two modes of transmission as σ changes. These results play an important role in the study of engineering disorder induction.

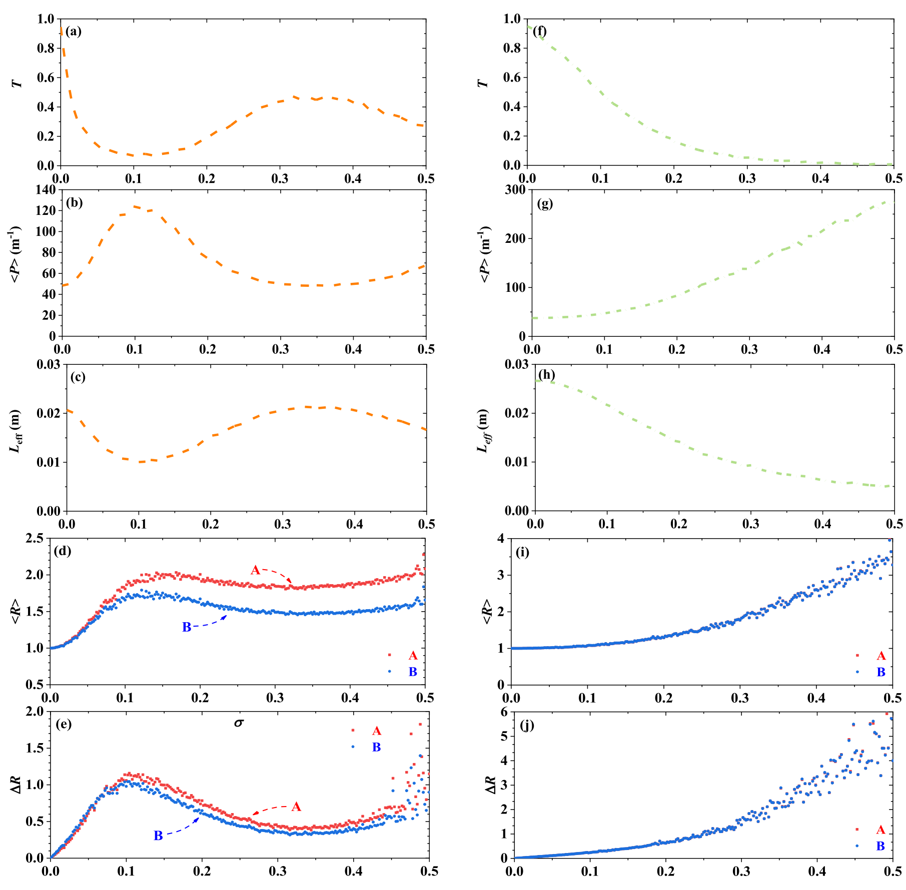

Fig. 8. Relationships between transmission T, inverse participation ratio <P>, effective propagation length L_{eff}, disorder-to-order energy ratio <R>, standard deviation of disorder-to-order energy ratio ΔR and disorder intensity σ at different angular frequencies, (a)~(e) $\omega = 1.219$ ($2\pi c/d$) and (f)~(i) $\omega = 1.351$ ($2\pi c/d$).

4. Conclusion

In summary, the disorder effect in the structure of CPCs is investigated, and the localization and delocalization properties of cylindrical waves in the structure can be artificially controlled through the modulation of disorder intensity. Four different transmission scenarios are explored by describing three different types of examples of disorder introduction. In the aforementioned four situations, the impacts of disorder introduction on the transmission state and electric field energy distribution are quantitatively investigated utilizing the inverse participation ratio, effective propagation length, disorder-to-order energy ratio, and its standard deviation. Based on the calculations, this study reveals the mechanism of how disorder affects structural transport mode. This work broadens the application scenario of disorder effects based on the CPCs to provide new insights into the design of various devices with EM wave transmission and localization requirements.

CRediT authorship contribution statement

Jia-Tao Zhang: Data curation, Formal analysis, Investigation, Writing – original draft, Visualization. **Si-Si Rao:** Software, Validation. **Hai-Feng Zhang:** Conceptualization, Methodology, Supervision, Writing – review & editing.

Declaration of competing interest

We would like to submit the manuscript entitled “Optical Propagation in Cylindrical Photonic Crystals with Engineered Disorder Effects”, which we wish to be considered for publication in this Journal. No conflict of interest exists in the submission of this manuscript, and the manuscript is approved by all authors for publication. I would like to declare on behalf of my co-authors that the work described was original research that has not been published previously, and not under consideration for publication elsewhere, in whole or in part. All the authors listed have approved the manuscript that is enclosed.

Data availability

Data will be made available on request.

References

[1] B. Reza, M. Ali, T. Reza, Design and simulation of a very fast and compact all-optical Full-Subtractor based on nonlinear effect in 2D photonic crystals, Opt. Quant. Electron. 53 (6) (2021) 351.
[2] S.R. He, Q. He, L.F. Wei, Atomic-type photonic crystals with adjustable band gaps, Opt Express 29 (2021) 43148–43163.
[3] J. Chen, J. Xie, E. Liu, B. Yan, J. Liu, Interface states in the rectangular lattice photonic crystals with identical dielectric rods, Results Phys. 23 (2021), 104082.
[4] S.R. Entezar, F. Ghasemi, S. Razi, Tunable resonant Bragg photonic bandgap structures based on active quantum dot layers; crystals with applications in all-optical switches manufacturing, Waves Random Complex Media 32 (2) (2020) 676–695.
[5] F. Ghasemi, S. Adinehpour, S. Razi, Single-step detection of toxic airborne metallic nanoparticles using Goos-Hänchen effect in photonic Bragg grating structures, Phys. Scripta 98 (8) (2023), 085507.
[6] M. Ahmed, M.A. Mazen, A.E. Hussein, 1D porous silicon photonic crystals comprising Tamm/Fano resonance as high performing optical sensors, J. Mol. Liq. 322 (2020), 114978.
[7] O.A. Yuriy, V.P. Yuriy, M.Y. Vladimir, Waves of a magnetoplasma solid-state cylinder under quasi-stationary conditions, IEEE Trans. Plasma Sci. 49 (10) (2021) 3078–3085.
[8] El-Naggar, Properties of defect modes in cylindrical photonic crystals, Optik 200 (2020), 163447.
[9] Q.Y. Wang, P.X. Wang, B.F. Wan, Y. Ma, H.F. Zhang, Study on the nonreciprocal absorption properties of cylindrical photonic crystals embedded in graphene cascaded by periodic and Rudin–Shapiro sequences at large incident angles, J. Appl. Phys. 129 (22) (2021), 223107.
[10] C. Xiong, J. Zhao, L. Wang, H. Geng, H. Xu, Y. Li, Trace detection of homologues and isomers based on hollow mesoporous silica sphere photonic crystals, Mater. Horiz. 4 (2017) 862–868.
[11] Michiel St, Rudolf S, Judith W, Mischa M, T Narayanan, Ad Lagendijk, Willem Lv, Inhibited light propagation and broadband reflection in photonic air-sphere crystals, Phys. Rev. Lett. 83 (14) (1999) 2730–2733.
[12] V.V. Nikolaev, G.S. Sokolovskii, M.A. Kaliteevskii, Bragg reflectors for cylindrical waves, Semiconductors 33 (1999) 147–152.
[13] C.A. Hu, C.J. Wu, T.J. Yang, S.L. Yang, Analysis of optical properties in cylindrical dielectric photonic crystal, Opt Commun. 291 (2013) 424–434.
[14] L. Qi, Z. Yang, F. Lan, X. Gao, Z. Shi, Properties of obliquely incident electromagnetic wave in one-dimensional magnetized plasma photonic crystals, Phys. Plasmas 17 (4) (2010), 042501.
[15] S. John, Strong localization of photons in certain disordered dielectric super lattices, Phys. Rev. Lett. 58 (23) (1987) 2486–2489.
[16] T. Yuan, T. Feng, Y. Xu, Manipulation of transmission by engineered disorder in one-dimensional photonic crystals, Opt Express 27 (5) (2019) 6483–6494.
[17] A.N. Poddubny, M.V. Rybin, F.L. Mikhail, Y.S. Kivshar, Fano interference governs wave transport in disordered systems, Nat. Commun. 3 (2012) 914.
[18] M. Elhanan, Y. Michael, F. Arkady, Y. Igor, K. Vladimir, H. Erez, Disorder-induced optical transition from spin Hall to random Rashba effect, Science 358 (6369) (2017) 1411–1415.
[19] I.D. Lev, D. Zaslavsky, A.A. Lisyansky, Statistics of the lyapunov exponent in 1D random periodic-on-average systems, Phys. Rev. Lett. 81 (24) (1998) 5390.
[20] M.A. Kaliteevski, D.M. Beggs, S. Brand, R.A. Abram, V.V. Nikolaev, Statistics of the eigenmodes and optical properties of one-dimensional disordered photonic crystals, Phys. Rev. 73 (5) (2006), 056616.
[21] M. Bellingeri, I. Kriegel, F. Scotognella, One dimensional disordered photonic structures characterized by uniform distributions of clusters, Opt. Mater. 39 (2015) 235–238.
[22] I.M. Vellekoop, A. Lagendijk, A.P. Mosk, Exploiting disorder for perfect focusing, Nat. Photonics 4 (2010) 320–322.
[23] G. Chen, H. Yu, The enlargement of high reflectance range in ultra-narrow bandpass filter with disordered one-dimensional photonic crystal, J. Appl. Phys. 115 (3) (2014) 1679.
[24] J.X. Li, Y. Xu, Q.F. Dai, S. Lan, S.L. Tie, Manipulating light–matter interaction in a gold nanorod assembly by plasmonic coupling, Laser Photon. Rev. 10 (5) (2016) 826–834.
[25] S. Yonatan, L. Eran, S. Mordechai, Disordered photonic time crystals, Phys. Rev. Lett. 126 (16) (2021), 163902.
[26] R. Satyam, G. Divya, J. Shuvendu, H.C. Carlos, N. Chittaranjan, V.U. Dinesh, Study of photonic band gap robustness in disordered polymer photonic crystals under hydrostatic pressure, Opt. Mater. 125 (2022), 112094.
[27] A.P. Jose, B. Farzaneh, B. Alvaro, G.M. Antonio, P. Carlos, I.M. Manuel, Cefe L. Fano-Like, Resonance from disorder correlation in vacancy-doped photonic crystals, Small (2023), 2302355.
[28] A.D. Mirlin, Statistics of energy levels and eigenfunctions in disordered systems, Phys. Rep. 326 (5–6) (2000) 259–382.